MTG-FCI: ATBD for Active Fire Monitoring Product

Doc.No. : EUM/MTG/DOC/10/0613
Issue : v2A e-signed
Date : 16 December 2019
WBS : MTG-834200

EUMETSAT
Eumetsat-Allee 1, D-64295 Darmstadt, Germany
Tel: +49 6151 807-7
Fax: +49 6151 807 555
http://www.eumetsat.int

Page left intentionally blank

This Document is Public

Change Record

Version	***Date***	***DCR* No.*** *if applicable*	***Description of Changes***
V1 draft	2010-12-10		For internal review
V1B	2011-01-17		First published version
V1C	2011-10-14		Second published version following the recommendations of the System PDR Science Panel
V2	2013-01-14		Editorial changes in sections 3.3 and 3.5.1 after external review and after the internal review of the MTG-FCI PGS
V2A	2019-12-16	692	Changed to adopt the latest version of the MSG FIR algorithm. Agreed at the MTG SYS CCB 001-20

****DCR = Document Change Request***

This Document is Public

Table of Contents

Table of Figures

Table of Tables

1 INTRODUCTION

1.1 Scope of this Document

This document describes the algorithm theoretical basis for the Active Fire Monitoring (FIR) product, as it shall be derived from the Meteosat Third Generation Flexible Combined Imager (MTG-FCI).

1.2 Applicable Documents

	Document Title	Reference
[AD-1]	MTG End Users Requirements Document	EUM/MTG/SPE/07/0036
[AD-2]	MTG Products in the Level-2 Processing Facility	EUM/C/70/10/DOC/08
[AD-3]	MTG-FCI: ATBD for Radiative Transfer Model	EUM/MTG/DOC/10/0382
[AD-4]	MTG-FCI: ATBD for Cloud Mask and Cloud Analysis Product	EUM/MTG/DOC/10/0542
[AD-5]	MSG ATBD for Active Fire Monitoring	EUM/RSP/DOC/20/1161774

1.3 Reference Documents

	Document Title	Reference
RD-1	Amraoui, M., C.C. DaCamara, J.M.C. Pereira, 2010: Detection and monitoring of African vegetation fires using MSG-SEVIRI imagery	Remote Sens Environ., 114, 1038-1052. doi:10.1016/j.rse.2009.12.019.
RD-2	Giglio L., J.D. Kendall, C.O. Justice, 1999: Evaluation of global fire detection algorithms using simulated AVHRR infrared data	Int. J. of Remote Sensing, Vol. 20, No. 10, pp. 1947-1985
RD-3	Giglio L., J. Descloitres, C.O. Justice, Y.J. Kaufman 2003: An Enhanced Contextual Fire Detection Algorithm for Modis.	Remote Sensing of Environment, Vol. 87, pp. 273-282
RD-4	Loveland T.R. and Belward A.S., 1997: The IGBP-DIS global 1km land cover data set, DISCover: first results.	Int. Journal of Remote Sensing, Vol. 18, No. 15, pp. 3289
RD-5	Morisette J.T., L. Giglio, I. Csiszar, C.O. Justice, 2005: Validation of the MODIS active fire product over Southern Africa with ASTER data.	Int. Journal of Remote Sensing, Vol. 26, No. 19, pp. 4239-4264
RD-6	Weaver J.F. and J.F. Purdom, 1995: Observing Forest Fires with the GOES-8, 3.9 µm Imaging Channel.	Weather and Forecasting, Vol. 10, pp. 803-808

1.4 Terminology

Acronyms and Abbreviations

Acronym/Abbr.	Explanation
AER	Aerosol Product
AMV	Atmospheric Motion Vectors
ASR	All Sky Radiance
ATBD	Algorithm Theoretical Basis Document
CMa	Cloud Mask
CRM	Clear Sky Reflectance Map
CT	Cloud Type
CTTH	Cloud Top Temperature and Height
FCI	Flexible Combined Imager
FCI-FDSS	FCI Full Disc Scanning Service
FCI-RSS	FCI Rapid Scanning Service
FDHSI	Full Disc High Spectral Resolution Imagery
FOR	Field of regard
GII	Global Instability Indices
HRFI	High Spatial Resolution Fast Imagery
HRV	High Resolution Visible Channel of SEVIRI
IR	Infrared
LUT	Lookup Table
MSG	Meteosat Second Generation
MTG	Meteosat Third Generation
NWP	Numerical Weather Prediction
OCA	Cloud Product (Optimal Cloud Analysis)
OLR	Outgoing Longwave Radiation
RTM	Radiative Transfer Model
RTTOV	Radiative Transfer for TOVS
SCE	Scene Identification
SAF	Satellite Application Facility
SEVIRI	Spinning Enhanced Visible and Infrared Imager
SSD	Spatial Sampling Distance
TIROS	Television and Infrared Observation Satellite
TOVS	TIROS Operational Vertical Sounder
TOZ	Total Column Ozone
VIS	Visible (solar)
VOL	Volcanic Ash Product

Definitions

Definition/Term	Explanation

Glossary of Terms Used in Equations

Variable Name	Explanation	Unit
a_1 to a_6	threshold coefficients	{various}
T_1 to T_6	threshold coefficients	{various}
B	Blackbody radiance according to Planck's Law	$mW/m^2/ster/cm^{-1}$
c	Speed of light	m/s
ch	channel index (here: IR 3.8 and IR 10.5)	n/a
h	Planck constant	J s
k	Boltzmann constant	J/K
$NCoast_{MTG}$	Distance to nearest coast line (for each pixel)	pixel
L_{down}	Downwelling radiance at surface level	$mW/m^2/ster/cm^{-1}$
L_{sol}	Solar radiance at the top of the atmosphere (IR 3.8)	$mW/m^2/ster/cm^{-1}$
L_{toa}	Radiance at top of atmosphere (for correct ε)	$mW/m^2/ster/cm^{-1}$
L_{top}	Radiance at top of atmosphere (for ε=1 surface)	$mW/m^2/ster/cm^{-1}$
$SType_{MTG}$	Pixel based surface type	n/a
$SType_{ECMWF}$	Surface type of ECMWF grid points	n/a
T	Temperature	K
T_B	Brightness temperature	K
T_{skin}	Surface skin temperature	K
ε	Emissivity	n/a
λ	Wavelength	µm
ρ	Reflectance in channel VIS 0.6	%
σ	Brightness temperature standard deviation	K
T_a	atmospheric transmittance	n/a
ζ_{glint}	Sun glint angle	deg
ζ_{sat}	Satellite zenith angle	deg
ζ_{sun}	Solar zenith angle	deg
$\zeta_{sun,thresh}$	Threshold solar zenith angle to define "night" conditions	Deg

1.5 Document Structure

Section 2 of this document provides a short overview over the MTG imaging instrument characteristics and the derived meteorological products, which will be referenced later in the text. This is followed by a detailed description of the underlying algorithm of the FIR product – its physical basis, the required input data, and a more detailed description of the product retrieval method. In section 4 an example of the FIR results is shown. Section 5 describes possible future developments of the FIR algorithm.

A full list of acronyms is provided in section 1.4, literature references are listed in the following section.

2 OVERVIEW

2.1 Relevant Instrument Characteristics

The mission of the Meteosat Third Generation (MTG) System is to provide continuous high spatial, spectral and temporal resolution observations and geophysical parameters of the Earth / Atmopshere System derived from direct measurements of its emitted and reflected radiation using satellite based sensors from the geo-stationary orbit to continue and enhance the services offered by the Second Generation of the Meteosat System (MSG) and its main instrument SEVIRI.

The meteorological products described in this document will be extracted from the data of the Flexible Combined Imager (FCI) mission. The FCI is able to scan either the full disc in 16 channels every 10 minutes with a spatial sampling distance in the range 1 – 2 km (Full Disc High Spectral Resolution Imagery (FDHSI) in support of the Full Disc Scanning Service (FCI-FDSS)) or a quarter of the earth in 4 channels every 2.5 minutes with doubled resolution (High spatial Resolution Fast Imagery (HRFI) in support of the Rapid Scanning Service (FCI-RSS)).

FDHSI and HRFI scanning can be interleaved on a single satellite (e.g. when only one imaging satellite is operational in orbit) or conducted in parallel when 2 satellites are available in orbit. Table 1 provides an overview over the FCI spectral channels and their respective spatial resolution.

The FCI acquires the spectral channels simultaneously by scanning a detector array per spectral channel in an east/west direction to form a swath. The swaths are collected moving from south to north to form an image per spectral channel covering either the full disc coverage or the local area coverage within the respective repeat cycle duration. Radiance samples are created from the detector elements at specific spatial sample locations and are then rectified to a reference grid, before dissemination to the End Users as Level 1 datasets. Spectral channels may be sampled at more than one spatial sampling distance or radiometric resolution, where the spectral channel has to fulfil FDHSI and HRFI missions or present data over an extended radiometric measurement range for fire detection applications.

Table 1: Channel specification for the Flexible Combined Imager (FCI)

Spectral Channel	*Central Wavelength, λ0*	*Spectral Width, Δλ0*	*Spatial Sampling Distance (SSD)*
VIS 0.4	0.444 µm	0.060 µm	1.0 km
VIS 0.5	0.510 µm	0.040 µm	1.0 km
VIS 0.6	0.640 µm	0.050 µm	1.0 km 0.5 km #1
VIS 0.8	0.865 µm	0.050 µm	1.0 km
VIS 0.9	0.914 µm	0.020 µm	1.0 km
NIR 1.3	1.380 µm	0.030 µm	1.0 km
NIR 1.6	1.610 µm	0.050 µm	1.0 km
NIR 2.2	2.250 µm	0.050 µm	1.0 km 0.5 km #1
IR 3.8 (TIR)	3.800 µm	0.400 µm	2.0 km 1.0 km #1
WV 6.3	6.300 µm	1.000 µm	2.0 km
WV 7.3	7.350 µm	0.500 µm	2.0 km
IR 8.7 (TIR)	8.700 µm	0.400 µm	2.0 km
IR 9.7 (O_3)	9.660 µm	0.300 µm	2.0 km
IR 10.5 (TIR)	10.500 µm	0.700 µm	2.0 km 1.0 km #1
IR 12.3 (TIR)	12.300 µm	0.500 µm	2.0 km
IR 13.3 (CO_2)	13.300 µm	0.600 µm	2.0 km

#1: The spectral channels VIS 0.6, NIR 2.2, IR 3.8 and IR 10.5 are delivered in both FDHSI sampling and a HRFI sampling configurations.

2.2 Generated Products

The agreed list of MTG-FCI Level 2 products is detailed in **Error! Reference source not found.** and is repeated here for easy reference:

1. **SCE**:
   Scene Identification (cloudy, cloud free, dust, volcanic ash, fire)
2. **OCA**:
   Cloud Product (cloud top height and temperature, cloud top phase, cloud top effective particle size, cloud optical depth, cloud sub-pixel fraction)
3. **ASR**:
   All Sky Radiance (mean IR radiance on a n x n pixel grid, together with other statistical information, for different scenes)
4. **CRM**:
   Clear Sky Reflectance Map (VIS reflectance for all non-absorbing channels, accumulated over time)
5. **GII**:
   Global Instability Indices (a number of atmospheric instability indices and layer precipitable water contents)
6. **TOZ**:
   Total Column Ozone
7. **AER**:
   Aerosol Product (asymmetry parameter, total column aerosol optical depth, refractive index, single scattering albedo, size distribution)
8. **AMV**:
   Atmospheric Motion Vectors (vector describing the displacement of clouds or water vapour features over three consecutive images, together with a vector height)
9. **OLR**:
   Outgoing Longwave Radiation (thermal radiation flux at the top of the atmosphere leaving the earth-atmosphere system)

The products will be derived from the spectral channel information provided by the FDHSI mission, on the resolution detailed in **Error! Reference source not found.**.

An important tool for product extraction is a radiative transfer model (RTM), as described in **Error! Reference source not found.**. The IR model choice for the Level 2 product extraction is RTTOV, which is developed and maintained by the Satellite Application Facility on Numerical Weather Prediction (NWP-SAF). An RTM for solar channels is likely to be product specific and is yet to be fully determined.

This ATBD describes the algorithm of the active fire monitoring product (FIR). The product will be derived over a certain processing area, defined as pixels lying within a great circle arc of pre-defined size around the subsatellite point (typically 70°).

3 ALGORITHM DESCRIPTION

3.1 Physical Basis Overview

The active fire monitoring product (FIR) derived from geostationary imager data is an important product to serve the environmental protection community.

Forest and vegetation fires have typical temperatures in the range of 500 K to 1000 K. According to Planck's law

$$B(\lambda,T) = \frac{2hc^2}{\lambda^5}\frac{1}{e^{\frac{hC}{\lambda kT}}-1} \quad \textbf{(1)}$$

B(λ,T): spectral radiance per unit solid angle for wavelength λ and temperature T
h: Planck constant
c: speed of light
k: Boltzmann constant

the peak emission of radiance for blackbody surfaces of such temperatures is between 3 and 5.8 µm (thus best observed by MTG-FCI channel IR 3.8). For an ambient temperature of 290 K, the peak of radiance emission is located at approximately 10 µm (corresponding to MTG-FCI channel IR 10.5). Figure 1 illustrates this concept.

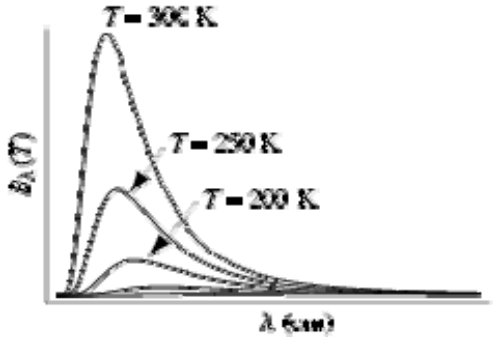

Figure 1: Graphical illustration of Planck's law for three different temperatures

This shift of peak emission goes together with a higher relative sensitivity to temperature changes towards smaller wavelengths. This is important, as typical wildfires are usually small "hot spots", much smaller than an MTG-FCI IR pixel. Such small fires have an only negligible effect on the IR 10.5 radiance, but a large effect in channel IR 3.8. The following example illustrates this:

> A temperature difference of the emitting surface of only 5 K at 300 K increases the radiance at 11 µm wavelength by ~ 7%.
> The same temperature difference, however, increases the radiance at 4 µm wavelength by ~18%.

Active fire detection algorithms from remote sensing use this shift of the peak emission and the increases sensitivity to temperature changes to detect such hot spots within a given pixel, which are usually fires of sub-pixel size. The sensitivity of the channel IR 3.8 to hot spots is so high that it shows small sub-pixel fires, which do not have any significant impact upon the IR 10.5 brightness temperature. Figure 2 shows a typical example of the respective MSG channels (IR 3.9 and IR 10.8).

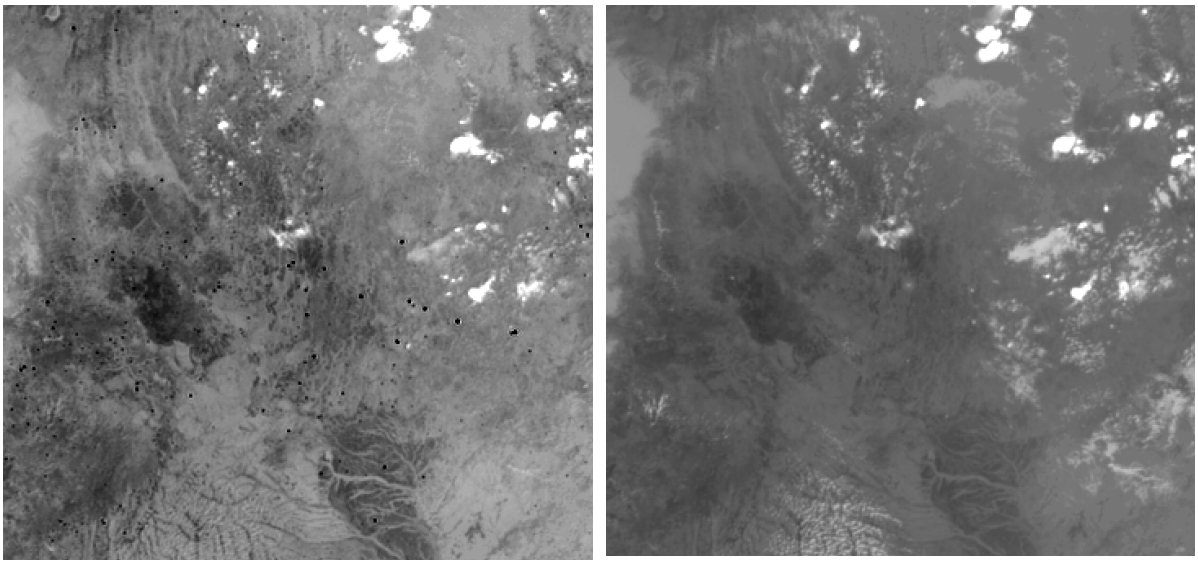

Figure 2: MSG examples of the IR 3.9 channel (left) and the IR 10.8 channel (right) for the same scene (29 July 2010, 1400 UTC over Central Africa). Wild fires are clearly visible in the IR 3.9 image as black hot spots.

However, the measurements in channel IR 3.8 are influenced by water vapour absorption, solar reflectance during day, and sub-pixel size clouds over hot surfaces.

The active fire detection algorithm aims at filtering out the active fires by a combination of threshold tests using channels IR 3.8 and IR 10.5. Both channels can be operated on a 2 km and a 1 km resolution, thus the algorithm needs to be in principle flexible to work on both resolutions.

The basic principles of the FIR algorithm are similar to those already in use for other instruments like GOES **Error! Reference source not found.**, AVHRR **Error! Reference source not found.**, and MODIS **Error! Reference source not found.**, and MSG **Error! Reference source not found.**.

The FIR algorithm shall only be applied to land surfaces, which means that off-shore oil burning fires or fires on small islands (e.g. active volcanoes which also fall under the hot spot category) are not monitored by the algorithm. Bare soil land surfaces are also excluded from the processing. Pixels are considered as bare soil, if the surface types are desert or open shrub land, where this classification is taken from climatological background information for the MTG-FCI field of view. In addition, the IR 10.5-IR 8.7 difference is used to check for bare soil: Because of a smaller IR 8.7 surface emissivity for bare soil compared to the IR10.5 emissivity, the difference of the two channels is high in these cases. It should be noted that

the active fire detection algorithm does not depend on the cloud mask, as the algorithm is trying to filter out hot spots, which are in general much warmer than clouds. This concept also allows detecting fires under semi-transparent clouds.

3.2 Assumptions and Limitations

The current fire monitoring algorithm is able to detect most of the existing active fires with a minimum of false alarms.

The following conditions, however, can still lead to falsely detected fires:

- Mixed water (river/lake/coast) and land scenes under sun glint conditions
- Unknown land surface emissivity, in particular over inhomogeneous terrain with spatially variant emissivity
- Dusk and dawn periods with rapidly changing IR 3.8 values (see section 3.5.2, thresholds for fire classification depend on day or night conditions and are ill-defined during dust and dawn).

Very small fires remain undetected due to the MTG-FCI radiometric performance. Examples of the general limitations for fire monitoring algorithms are given by **Error! Reference source not found.**

3.3 Algorithm Basis Overview

For the processed pixels, the FIR algorithm uses the following criteria to check for potential fire and fire pixels:

(1) Brightness temperature of channel IR 3.8 has to exceed a certain threshold
(2) Brightness temperature difference of channels IR 3.8 and IR 10.5 has to exceed a certain threshold
(3) Difference of the standard deviations of channel IR 3.8 and IR 10.5 has to exceed a certain threshold

(The standard deviations are computed over a 3x3 pixel group, centred on the processing pixel)

Test (1):
This test identifies pixels with much warmer than expected IR 3.8 temperatures. Section 3.5.2 will explain how the "expected" IR 3.8 temperatures are derived.

Test (2):
As channel IR 10.5 is much less sensitive to hot spots, the brightness temperature of IR 10.5 will not be as high as the brightness temperature in channel IR 3.8. This means that the brightness temperature difference of channels IR 3.8 and IR 10.5 is also higher than for non-fire pixels.

Test (3):

The difference of the standard deviation of channel IR 3.8 and the standard deviation of channel IR 10.5 over 3 x 3 pixels around a central hot spot is used to identify the real hot spot versus the natural (heated) background temperature of the surface. For active fires it is expected that the standard deviation for channel IR 3.8 is much larger than for channel IR 10.5. For other clear surfaces the standard deviation in both channels are approximately the same, while for clouds and cloud edges the standard deviation for channel IR 10.5 is larger than for channel IR 3.8.

The standard deviation is calculated on a 3x3 pixel array around each MTG-FCI pixel.

3.4 Algorithm Input

Table 2 lists the data that needs to be available at the start of the FIR processing.

3.4.1 Primary Sensor Data

For each pixel within the processing area, the brightness temperatures for the three IR MTG-FCI channels and the VIS 0.6 channel, as listed in Table 2, must be available. The pixel resolution of the channel with the lowest resolution (i.e. IR 8.7, 2 km resolution) determines the resolution of the product. This means that the VIS 0.6 channel (1 km resolution) needs to be averaged to the coarser resolution.

Table 2: Necessary input data for the FIR processing

Parameter Description	Variable Name
Reflectances for MTG-FCI channel VIS0.6 for each pixel within the processing area	ρ
Brightness Temperatures for channels IR 3.8, IR 8.7, IR 10.5, for each pixel within the processing area	$T_B(ch)$[1]
Solar zenith and satellite zenith angles for each pixel within the processing area	ζ_{sun}, ζ_{sat}
Surface emissivity information, for the same three channels, for each pixel over the processing area	$\varepsilon(ch)$
Sun glint angle	ζ_{glint}
Radiances derived with RTTOV from ECMWF forecasts, interpolated to the image processing time. Needed RTTOV parameters: - Top of atmosphere clear sky radiance - Total transmittance - Downward radiance at surface level for channels IR3.8 and IR10.5	 $r_{top}(ch)$ $\tau_a(ch)$ $r_{down}(ch)$
Surface type information for each MTG-FCI pixel (land type, or sea)	$SType_{MTG}$

Surface type information for the ECMWF grid points within the processing area (land or sea)	$SType_{ECMWF}$

[1]: index (ch) refers to channels IR 3.8, IR 10.5

3.4.2 Ancillary Dynamic Data

The FIR product needs the RTTOV output, as stated in Table 2, interpolated to the pixel position from the adjacent RTTOV grid points:

For RTTOV-9, these are the parameters:

$r_{top}(ch)$ *radiance % clear* (for all relevant channels, in the "radiance type" RTTOV output)

$\tau_a(ch)$ *transmission % tau_total* (for all relevant channels, in the "transmission type" RTTOV output)

$r_{down}(ch)$ *radiance % dnclear* (for all relevant channels, at the lowest atmospheric level, in the "radiance type" RTTOV output)

As RTTOV provides the results on the ECMWF grid (which typically has a fixed latitude and longitude spacing), the results need to be interpolated to the pixel position:
Within the spatial interpolation of the ECMWF profiles, care has to be given to the actual surface type value of the forecast points compared to the (predominant) surface type of the FoR. Only such ECMWF grid points shall be used for the spatial interpolation, which have the same surface type (only land/sea are discriminated as two possible types).
If, for example, a specific FoR has surface type “land”, but a number of the surrounding ECMWF grid points have surface type “sea” (or vice versa), these grid points shall be disregarded in the spatial interpolation. Otherwise, coastal features will wrongly show up in the final product. Figure 3 shows a schematic of this process.
In case, however, that all surrounding ECMWF grid points differ in their surface type from the pixel's surface type (e.g. small islands or small lakes or rivers), all four surrounding grid points have to be used.

Figure 3: ***Schematic illustration of the use of forecast data depending on the FoR and the forecast grid surface type. Only the forecast data of the same surface type shall be used, as illustrated for the "land" case (top) and the "sea" case (bottom). The arrows denote which ECMWF grid points shall be used in these cases.***

3.4.3 Ancillary Static Data

FIR uses the following ancillary static datasets:

- Pixel-based land-sea-mask/surface-type-map
- Pixel-based emissivity maps for the three infrared channels IR 3.8 and IR 10.5

The pixel-based land-sea-mask/surface-type-map consists of 17 different land surface types one ocean/open water surface type and one mixed water/land surface type. This map can be e.g. derived from the International Geosphere-Biosphere Programme (IGBP) surface type map **Error! Reference source not found.**.

The pixel-based emissivity data is expected to be constant over a certain period (typically a month), so the processing has to allow for a possible time dependence in this input dataset.

3.5 Detailed Description

The algorithm calculates a fire probability based on simple threshold tests. This fire probability is used to distinguish between fires of low, mid or high confidence (see section 3.5.1). However, the fire probability parameter will allow the users to decide on their own balance between Detection Efficiency and False Alarm Rate.

The FIR algorithm will be applied if the following conditions are all met:

- Pixel is land (not water or mixed water/land surface type)
- Pixel is not bare soil:
  This information is taken from the pixel based surface type mask $SType_{MTG}$; in addition the brightness temperature difference IR 8.7 – IR 10.5 needs to be smaller than 4 K
- During day the reflectance ρ in channel VIS 0.6 is smaller than 15% (to exclude bare soil and small clouds)
- The sun glint angle ζ_{glint} is larger than 3º.
- The brightness temperature of channel IR10.5 is larger than a threshold (threshold0)

3.5.1 Description of the Threshold Tests

The fire detection is based on a fire probability calculation, which is performed as follows:

Prob1 = MAX(0., MIN(1., (T39 – threshold1) / (threshold2 – threshold1)))
Prob2 = MAX(0., MIN(1., ((T39 – T10.8) – threshold3) / (threshold4 – threshold3)))
Prob3 = MAX(0., MIN(1., ((StDev39 – StDev10.8) – threshold5) / (threshold6 – threshold5)))

FIRProb = Prob1*Prob2*Prob3

If FIRProb is 0. the processing for the pixel is stopped here with the result “no fire”. Otherwise the processing is continued as follows:

A fire with FIRProb larger or equal prob_threshold1 (currently 0.8) is considered as fire with high confidence.
A fire with FIRProb smaller than prob_threshold1 (currently 0.8) and higher or equal prob_threshold2 (currently 0.4) is considered as fire with medium confidence.
A fire with FIRProb smaller than a prob_threshold2 (currently 0.4) and higher or equal prob_threshold3 (currently 0.2) is considered as fire with low confidence.
However users may still use pixels with a probability higher than 0 and lower than 0.2 for their own purposes and considerations.

3.5.2 Derivation of the Thresholds

As the brightness temperatures in the infrared channels change in the course of a day, and as the IR 3.8 channel has a solar contribution, which also changes during the day, the thresholds 1-9 as mentioned in section 3.5.1 are not fixed values, but are also defined such that they model the diurnal temperature cycle, i.e. the thresholds are dynamic.

In order to derive these dynamic thresholds, the algorithm uses the RTTOV results. As RTTOV uses unit emissivity values for all grid-points, the given top of the atmosphere clear sky radiance has to be corrected for the given (pixel-based) land surface emissivity. The emissivity corrected radiances for channels IR 3.8 and IR 10.5 consist of

(a) The emission of the surface, multiplied by the atmospheric transmission of the entire atmosphere:

$$\varepsilon(ch)\, B_{ch}(T_{skin})\, T_a(ch)$$

$\varepsilon(ch)$:	emissivity for channel ch
$B_{ch}(T_{skin})$:	the spectral blackbody radiance for channel c for the surface skin temperature T_{skin}
$T_a(ch)$	total atmospheric transmittance for channel ch

(b) Downwelling radiation reflected by the surface

$$(1-\varepsilon(ch))\, L_{down}(ch)\, T_a(ch)$$

$(1-\varepsilon(ch))$:	surface reflectivity for channel ch
$L_{down}(ch)$:	downwelling radiance at surface level, for channel ch
$T_a(ch)$:	total atmospheric transmittance for channel ch (as above)

(c) Contribution from the atmosphere above the surface, which can be inferred from

$$L_{top}(ch) - B_{ch}(T_{skin})\,T_a$$

$L_{top}(ch)$: total outgoing radiance at the top of the atmosphere for channel ch
$B_{ch}(T_{skin})$: spectral blackbody radiance for channel ch for the surface skin temperature T_{skin}, as above
T_a (ch) total atmospheric transmittance for channel ch, as above

(d) In addition, for channel IR 3.8, its solar component needs to be considered according to

$$(1-\varepsilon(IR\,3.8))\,L_{sol}(IR\,3.8)\cos(\zeta_{sun})\,T_a(IR\,3.8)\,T_a(IR\,3.8)$$

during daylight hours, while the solar contribution is of course 0 at night.

[1-ε(IR 3.8)]: surface reflectivity in channel IR 3.8
L_{sol}(IR 3.8): solar radiance at the top of the atmosphere, convolved with the IR 3.8 spectral response
ζ_{sun}: local solar zenith angle
T_a (IR 3.8): total atmospheric transmittance for channel IR 3.8

In summary, the IR 10.5 top of atmosphere radiance, corrected for the local surface emissivity, is

$$\begin{aligned} L_{toa}(IR\,10.5) = {} & \varepsilon(IR\,10.5)\,B_{IR\,10.5}(T_{skin})\,T_a(IR\,10.5) + \\ & (1-\varepsilon(IR\,10.5))\,L_{down}(IR\,10.5)\,T_a(IR\,10.5) + \\ & L_{top}(IR\,10.5) - B_{IR\,10.5}(T_{skin})\,T_a(IR\,10.5) \end{aligned} \qquad \textbf{(2)}$$

and for channel IR 3.8, the corrected radiance is

$$\begin{aligned} L_{toa}(IR\,3.8) = {} & \varepsilon(IR\,3.8)\,B_{IR3.8}(T_{skin})\,T_a(IR\,3.8) + (1-\varepsilon(IR\,3.8))\,L_{down}(IR\,3.8)\,T_a(IR\,3.8) + \\ & L_{top}(IR\,3.8) - B_{IR\,3.8}(T_{skin})\,T_a(IR\,3.8) + \\ & (1-\varepsilon(IR\,3.8))\,L_{sol}(IR\,3.8)\cos(\zeta_{sun})\,T_a(IR\,3.8)\,T_a(IR\,3.8) \end{aligned} \qquad \textbf{(3)}$$

The following parameters are available from the RTTOV output (interpolated in time and to the respective pixel position), reference is RTTOV version 9:

transmission % tau_total(ch)	representing T_a (ch)
radiance % clear(ch)	representing $L_{top}(ch)$ for ε = 1
radiance % dnclear(ch)	representing $L_{down}(ch)$

L_{sol}(IR 3.8) must be pre-computed from the solar spectrum and the IR 3.8 spectral response function (and should be weighted with the actual earth-sun distance).

The respective emissivities, the solar zenith angle and the surface skin temperature must be valid for the processed pixel for the corresponding acquisition time. These final radiances are then converted to brightness temperatures (for details on the radiance to brightness temperature conversion, see **Error! Reference source not found.**, section 3.2), providing the

"expected" or "predicted" brightness temperatures for the processed pixel, T_{pred_39} and T_{pred_108} .. The final thresholds depend on these predicted temperatures according to:

$$\text{Threshold0} = (T_{pred\_105} + a0)$$
$$\text{Threshold1} = \text{MAX}(T_1 , (T_{pred\_39} + a1 * (1. + \sin(\zeta_{sat}))))$$
$$\text{Threshold2} = \text{MIN}(T_2 , (T_{pred\_39} + a2 * (1. + \sin(\zeta_{sat}))))$$
$$\text{Threshold3} = \text{MAX}(T_3 , ((T_{pred\_39} - T_{pred\_108}) + a3 * (1. + \sin(\zeta_{sat}))))$$
$$\text{Threshold4} = \text{MIN}(T_4 , ((T_{pred\_39} - T_{pred\_108}) + a4 * (1. + + \sin(\zeta_{sat}))))$$
$$\text{Threshold5} = T_5 + a5 * (1. + \sin(\zeta_{sat})))$$
$$\text{Threshold6} = T_6 + a6 * (1. + \sin(\zeta_{sat})))$$

It should be noted that this approach is only valid for satellite zenith angles ζ_{sat} up to 70°.

The coefficients a_0 to a_6 and T_1 to T_6 are highly empirical: Values for MSG-SEVIRI exist, which will need fine tuning for MTG-FCI. In addition, the coefficients are different for "day" and "night". In this context, "day" is defined for cases where

$$\zeta_{sun} < \zeta_{sun,thresh}$$

where $\zeta_{sun,thresh}$ is a certain cut-off solar zenith angle (e.g. 85°). "night" is defined for cases where

$$\zeta_{sun} > 90°$$

For cases where

$$\zeta_{sun,thresh} \leq \zeta_{sun} \leq 90°$$

the values of the coefficients need to be linearly interpolated between their respective day and night value. The current version of the coefficients a_0 to a_6 and T_1 to T_6 exists for MSG, (see Table 3). The fine-tuning of the corresponding MTG-FCI values will be done during the commissioning phase of MTG-FCI.

Table 3: Coefficients a_1 to a_6 and T_1 to T_6 for MSG

Coeff	Day	Night
a0	-3.0	-3.0
T1	280	275
a1	0	0
T2	335	330
a2	5	5
T3	0	0
a3	0.5	0.5
T4	4	2
a4	2	2
T5	0	0
a5	0.5	0.5
T6	2	2
a6	2	2

Note: some coefficients are set to zero, thus having no effect, but might be useful after further tuning

3.6 Output Description

For each pixel the FIR output will contain the probability factor and the information whether the pixel has no fire, or a fire with the appropriate confidence level.

Table 4: FIR output parameter

Parameter	**value**	**Meaning**
Fire type	0	No fire
	1	Fire low confidence
	2	Fire mid confidence
	3	Fire high confidence
Fire propability	0 – 100 %	Fire propability

4 RESULTS

As an example, the algorithm was applied to Meteosat-11 data of July 2018. During this period there were major fires over Greece which had not been detected by the old version of the FIR algorithm. The result for 23rd July 2018 11 UTC is shown in Figure 4.

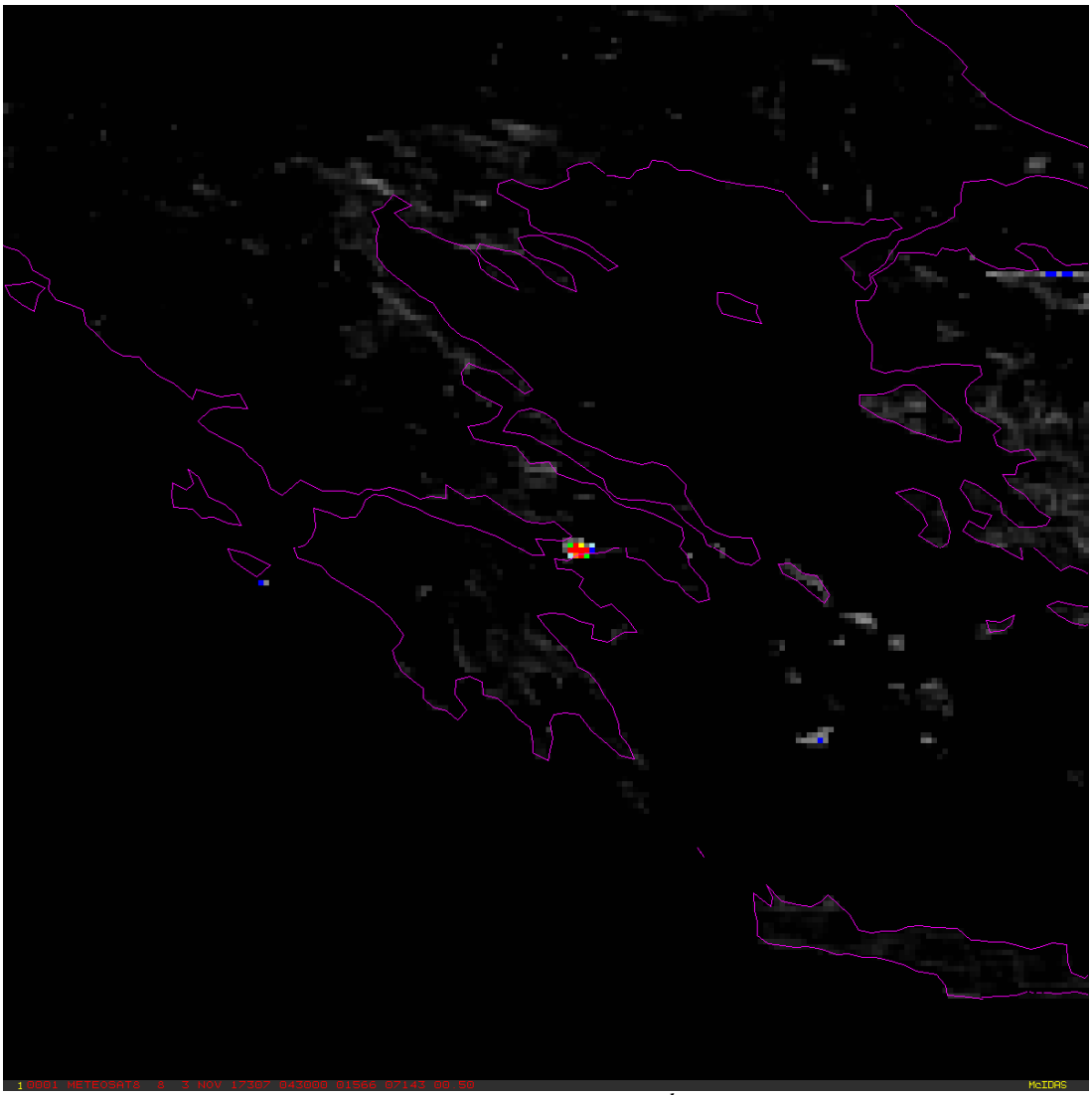

Figure 4: Fire detection over Greece on 23rd 11 UTC (Kineta fire case).

The figure 4 shows the fire probability in the following colour coding:
Red – FIRProb > 0.9,
Orange – FIRProb > 0.8,
Yellow – FIRProb > 0.7,
Green – FIRProb > 0.6,
Turquoise – FIRProb > 0.5,
Blue – FIRProb >0.4
Grey – FIRProb < 0.4

In the following table 5 a typical example for the FIR results of the new algorithm for a midday image (22 August 2019) over the MSG FOV is illustrated:

Table 5: Fire probability for the 12 UTC image on 22nd August 2019

Fire probability	**Number of fire pixels**	**Fire class**
Prob > 80%	1065	High confidence
80% > Prob > 40%	1397	Mid confidence
40% > Prob > 20%	2383	Low confidence
20% > Prob > 10%	3784	
10% > Prob > 0%	20320	

5 FUTURE DEVELOPMENTS

The above description assumes an overall pixel resolution of 2 km for the channels VIS 0.6, IR 3.8, IR 8.7 and IR 10.5. As VIS 0.6, IR 3.8 and IR 10.5 will be all available on a 1 km resolution, the algorithm can in principle also be applied to this resolution: This will have the advantage of detecting more (smaller) fires. The only difference to the 2 km version is the use of the IR 8.7 channel: As outlined in section 3.5, this channel is only used to detect bare soil (through the brightness temperature difference IR 10.5 and IR 8.7) – this bare soil check can, however, also be done through the detailed surface type map and (during daytime) through the use of the VIS 0.6 channel.

In addition the use of channels NIR1.6 and NIR2.2 has to be considered.

Furthermore, section 3.5. states that the algorithm should be run over land pixels only: In principle, the algorithm will also work over sea areas and over mixed land/water pixels, so a full disk application may be considered for MTG-FCI.

During the commissioning phase of MTG-FCI, the coefficients a_1 to a_6 and T_1 to T_6 need to be fine-tuned to account for possible spectral differences between MSG and MTG-FCI.
In addition the thresholds need to be fine-tuned during the commissioning phase of MTG-FCI.

Additional tests to filter out false alarms (e.g. standard deviation of the difference (IR3.8-IR10.5) may also be tested.